

Disentangled Representation Learning via Flow Matching

Jinjin Chi^{1,2} Taoping Liu¹ Mengtao Yin¹ Ximing Li¹ Yongcheng Jing² Dacheng Tao²

Abstract

Disentangled representation learning aims to capture the underlying explanatory factors of observed data, enabling a principled understanding of the data-generating process. Recent advances in generative modeling have introduced new paradigms for learning such representations. However, existing diffusion-based methods encourage factor independence via inductive biases, yet frequently lack strong semantic alignment. In this work, we propose a flow-matching-based framework for disentangled representation learning, which casts disentanglement as learning factor-conditioned flows in a compact latent space. To enforce explicit semantic alignment, we introduce a non-overlap (orthogonality) regularizer that suppresses cross-factor interference and reduces information leakage between factors. Extensive experiments across multiple datasets demonstrate consistent improvements over representative baselines, yielding higher disentanglement scores as well as improved controllability and sample fidelity.

1. Introduction

Disentangled representation learning has emerged as a fundamental objective in modern machine learning, playing a pivotal role in advances across computer vision, natural language processing (NLP), and reinforcement learning (Bengio et al., 2013; Wang et al., 2024). Motivated by the observation that the physical world is governed by a set of independent underlying factors, such as object shape, color, and size, this paradigm aims to encode high-dimensional observations into compact latent representations in which these semantic factors are explicitly separated. As illustrated in Figure 1, a single observation can be explained by multiple distinct factors of variation, here exemplified by

¹College of Computer Science and Technology, Jilin University, Changchun, China ²College of Computing and Data Science, Nanyang Technological University, Singapore. Correspondence to: Ximing Li <liximing86@gmail.com>.

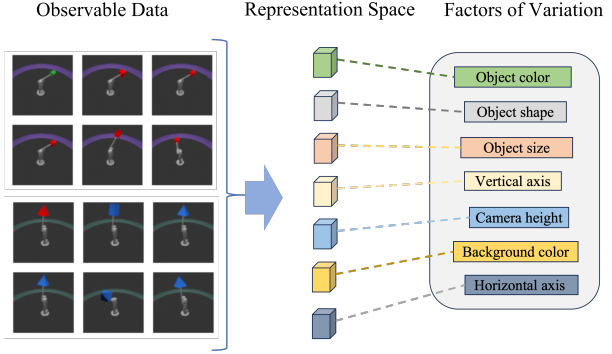


Figure 1. Illustration of the MPI3D-toy dataset (Gondal et al., 2019). The seven rectangles represent the underlying factors of variation in the scene, including object color, shape, size, camera height, background color, vertical axis and horizontal axis. Disentangled representation learning aims to encode these distinct generative factors into independent latent variables within the learned representation space.

seven interpretable generative factors. Such structurally disentangled representations provide a powerful inductive bias for downstream tasks, enabling controllable image synthesis and editing in vision (Xu et al., 2023; Wang et al., 2023), facilitating style manipulation and semantic control in NLP (Cheng et al., 2020; Hu et al., 2022), and supporting robust policy generalization and transfer in robotics (Higgins et al., 2018; Wu et al., 2025). Consequently, disentangled representation learning has become an active and rapidly growing area within representation learning.

A wide range of disentangled representation learning methods have been proposed to advance this line of research. Among them, generative modeling-based methods have demonstrated particular effectiveness in learning disentangled representations from high-dimensional image data, owing to their ability to explicitly model the data generation process. On the one hand, Variational Autoencoder (VAE)-based methods, such as β -VAE (Higgins et al., 2017) and FactorVAE (Kim & Mnih, 2018), encourage disentanglement by imposing structural regularization on the latent space. However, these methods suffer from a trade-off between reconstruction fidelity and disentanglement strength (Chen et al., 2018; Burgess et al., 2018). On the other hand, Generative Adversarial Network (GAN)-based methods, including InfoGAN (Chen et al., 2016), InfoGAN-CR

(Lin et al., 2020) pursue disentanglement from a different perspective, typically by inducing semantic structure through controllable latent variables. Despite their remarkable generative capability, GAN-based models generally lack a reversible inference mechanism between data and latent spaces, which makes them less flexible than VAEs for representation learning (Wang et al., 2024).

More recently, modern generative models, particularly diffusion models, have attracted increasing attention due to their strong modeling capacity and stable training dynamics, opening new opportunities for disentangled representation learning. Existing diffusion-based methods (Wu & Zheng, 2024; Yang et al., 2023b; 2024; Jun et al., 2025) commonly introduce inductive biases to diffusion models to encourage statistical independence across latent dimensions (Jun et al., 2025). However, disentanglement in practice requires not only independence but also a semantic alignment criterion: *each latent unit (or subspace) should correspond to a distinct, interpretable generative factor*. When semantic alignment is weak, latent dimensions may remain statistically decorrelated yet still mix factors, limiting interpretability and undermining fine-grained, factor-wise interventions.

To address these limitations, we argue that the deterministic formulation of *flow matching* provides a more principled geometric basis for semantic alignment than stochastic diffusion trajectories. Flow matching learns continuous-time generative dynamics by directly matching probability flow fields, thereby avoiding iterative denoising objectives and the associated noise-schedule design choices, while enabling efficient inference via Ordinary Differential Equation (ODE). Building on these structural advantages, we develop a flow-matching framework for disentangled representation learning that encourages factor-specific, non-overlapping latent transformations and provides explicit semantic alignment. To the best of our knowledge, this is the first study to investigate flow matching for disentanglement in this setting. Our key contributions are three-fold:

- *Flow-matching formulation for disentanglement.* We cast disentangled representation learning as learning a factor-conditioned flow in a compact latent space, enabling a deterministic and effective generative process with ODE-based sampling.
- *Alignment module via factor-aligned vector-field decomposition.* We propose an alignment module that enforces explicit semantic alignment by decomposing the learned vector field into factor-specific components, yielding a direct mapping from factors to latent-space dynamics and enabling fine-grained, factor-level control within the flow-matching framework.
- *Empirical superiority across datasets and metrics.* Extensive experiments on multiple datasets demonstrate

that our method consistently outperforms representative baselines, yielding quantitative improvements in disentanglement metrics (e.g., DCI and FactorVAE scores) and qualitative gains in semantic controllability and sample fidelity.

2. Related Work

VAE-based methods. VAEs (Kingma & Welling, 2014) are deep probabilistic generative models trained via variational inference to model complex data distributions. By introducing latent variables and maximizing the evidence lower bound (ELBO), VAEs jointly learn an approximate posterior for inference and a decoder for image generation. With appropriate regularization, VAEs have been shown to learn disentangled latent representations on relatively simple datasets. For instance, β -VAE (Higgins et al., 2017) encourages factorized latent variables by up-weighting the Kullback–Leibler (KL) divergence term in the ELBO, thereby increasing the pressure toward a simple prior and promoting independence among latent dimensions. Building on this idea, FactorVAE (Kim & Mnih, 2018) explicitly penalizes the total correlation of the aggregated posterior to better isolate independent generative factors, while β -TCVAE (Chen et al., 2018) further decomposes the KL term and directly controls the contribution of total correlation. Other variants, such as DIP-VAE (Kumar et al., 2018), match moments of the aggregated posterior to those of the prior to encourage disentanglement without severely degrading reconstruction quality. In essence, these methods modify the standard VAE objective by reweighting ELBO components or introducing additional regularizers, aiming to balance reconstruction fidelity with the statistical independence and interpretability of learned representations.

GAN-based methods. GAN-based methods provide an alternative route to disentangled representation learning by leveraging adversarial training to match the generated and real data distributions (Goodfellow et al., 2014). A representative method is InfoGAN (Chen et al., 2016), which augments the standard GAN objective with a mutual-information regularizer between a subset of latent codes and the generated samples, encouraging these codes to capture salient and interpretable factors of variation. Subsequent extensions further improve controllability and disentanglement by imposing structured latent spaces or explicit factorization constraints, e.g., through separating “content” and “style” codes (Kazemi et al., 2019; Varur et al., 2025). In addition, StyleGAN and its variants demonstrate that architectural inductive biases, such as mapping networks and modulation-based synthesis, can lead to semantically meaningful, partially disentangled control over attributes at different layers, enabling high-quality and controllable image generation (Karras et al., 2019; 2020). However, GAN-based methods

often face challenges in reconstruction, since accurate recovery of latent codes from real images (GAN inversion) remains difficult in practice (Wang et al., 2022).

Diffusion-based methods. Diffusion models have recently emerged as a dominant family of generative models, achieving state-of-the-art fidelity and mode coverage by learning to reverse a gradual noising process, or equivalently, by estimating the score function of the data distribution (Ho et al., 2020; Yang et al., 2023a). Unlike VAEs and GANs, diffusion-based disentanglement remains relatively underexplored because diffusion architectures do not naturally yield a compact, factorized latent representation. Consequently, the limited number of existing methods typically rely on strong inductive biases into diffusion models to enforce factor-wise independence (Wu & Zheng, 2024; Yang et al., 2023b; 2024; Jun et al., 2025). Specifically, (Wu & Zheng, 2024) imposes visual interpretability by decomposing images into separate content and mask groups to uncover visual concepts; (Yang et al., 2023b) structures the denoising pathway to separate factors by enforcing constraints across all diffusion time steps; (Yang et al., 2024) exploits cross-attention mechanisms to route distinct factors into disentangled representations; and (Jun et al., 2025) further enhances separation via dynamic Gaussian anchoring. Despite these advances, such methods remain fundamentally constrained by the stochastic nature of diffusion trajectories and the complexity of iterative denoising, which not only incur high computational costs but also lack the deterministic geometric structure required to strictly enforce precise semantic alignment.

3. Background

Let $p_0(\mathbf{x})$ denote a tractable source distribution (typically a standard Gaussian) and let $p_1(\mathbf{x})$ denote the target data distribution. Flow matching is a simulation-free generative modeling framework that learns a time-dependent vector field to transport probability mass from p_0 to p_1 (Lipman et al., 2022).

Probability flow ODE. Let $\mathbf{v}_t : \mathbb{R}^d \rightarrow \mathbb{R}^d$ be a time-dependent vector field for $t \in [0, 1]$. Under mild regularity conditions, \mathbf{v}_t defines a deterministic flow map ϕ_t as the solution to the Ordinary Differential Equation (ODE),

$$\frac{d}{dt}\phi_t(\mathbf{x}) = \mathbf{v}_t(\phi_t(\mathbf{x})), \quad \phi_0(\mathbf{x}) = \mathbf{x}. \quad (1)$$

Starting from an initial draw $\mathbf{x}_0 \sim p_0$, the ODE generates a trajectory $\mathbf{x}_t = \phi_t(\mathbf{x}_0)$. The distribution of \mathbf{x}_t is therefore the pushforward of p_0 through ϕ_t ,

$$q_t := (\phi_t)_\# p_0. \quad (2)$$

In generative modeling, we parameterize the vector field \mathbf{v}_t by a neural network $\mathbf{v}_\theta(\mathbf{x}, t)$ and aim to choose θ so that

transporting p_0 to time $t = 1$ matches the data distribution, i.e., $q_1 \approx p_1$. At inference time, we sample $\mathbf{x}_0 \sim p_0$ and numerically integrate Eq. (1) from $t = 0$ to 1 to obtain \mathbf{x}_1 .

Conditional Flow Matching (CFM). Directly matching q_1 to p_1 is typically intractable. Conditional Flow Matching (CFM) (Lipman et al., 2022) instead trains \mathbf{v}_θ using supervised regression targets constructed from pairs of endpoint samples. Concretely, we independently draw $\mathbf{x}_0 \sim p_0$ and $\mathbf{x}_1 \sim p_1$, then sample a time $t \sim \mathcal{U}[0, 1]$ and define an interpolation (a “bridge”) between the endpoints,

$$\mathbf{x}_t = \psi_t(\mathbf{x}_0, \mathbf{x}_1). \quad (3)$$

The key observation is that ψ_t induces a *conditional* velocity along this bridge,

$$\mathbf{u}_t := \frac{d}{dt}\psi_t(\mathbf{x}_0, \mathbf{x}_1), \quad (4)$$

which can be computed analytically once ψ_t is chosen. CFM trains the model to predict this velocity from the intermediate point \mathbf{x}_t and time t by minimizing

$$\mathcal{L}_{\text{CFM}}(\theta) = \mathbb{E}_{\mathbf{x}_0, \mathbf{x}_1, t} \left[\left\| \mathbf{v}_\theta(\mathbf{x}_t, t) - \mathbf{u}_t \right\|_2^2 \right]. \quad (5)$$

Intuitively, this objective encourages \mathbf{v}_θ to agree with the local direction of transport implied by the chosen bridge between source and data samples, without requiring explicit likelihood evaluation or solving an optimal transport problem (Dao et al., 2023).

Linear interpolation. In this work, we use the simple linear bridge

$$\mathbf{x}_t = (1 - t)\mathbf{x}_0 + t\mathbf{x}_1, \quad (6)$$

which yields a constant velocity with respect to t . Differentiating Eq. (6) gives

$$\mathbf{u}_t = \frac{d}{dt}\mathbf{x}_t = \mathbf{x}_1 - \mathbf{x}_0. \quad (7)$$

Plugging Eq. (7) into the generic CFM objective in Eq. (5) results in the training loss used in our method,

$$\mathcal{L}_{\text{Linear}}(\theta) = \mathbb{E}_{\mathbf{x}_0, \mathbf{x}_1, t} \left[\left\| \mathbf{v}_\theta(\mathbf{x}_t, t) - (\mathbf{x}_1 - \mathbf{x}_0) \right\|_2^2 \right]. \quad (8)$$

4. Our Method

In this work, we propose a disentangled representation learning framework based on a *factor-conditioned* latent-space flow. Given an input image, we extract N factor embeddings, each intended to summarize a distinct, controllable semantic attribute. We then learn a conditional flow in latent space that transports samples from a simple source prior to the data distribution. Crucially, we parameterize the flow

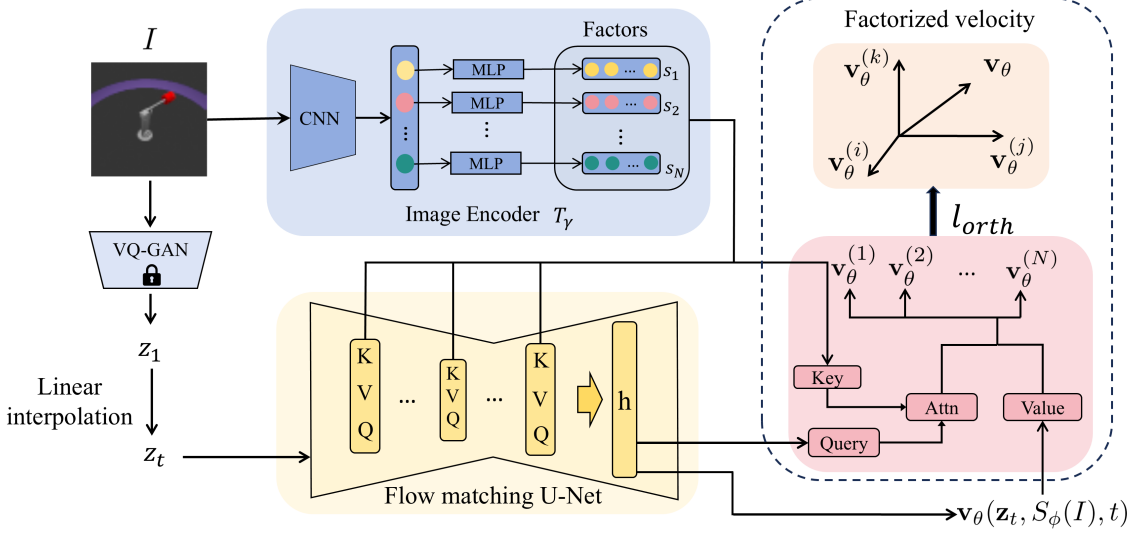


Figure 2. Illustration of our proposed framework. Given an input image I , an image encoder T_γ extracts a set of factor representations, which serve as conditional inputs to the flow-matching model via cross-attention. The right panel illustrates the *Factorized Velocity via Output Attention* module, which decomposes the predicted velocity field into factor-specific components and enforces non-overlapping, semantically aligned latent dynamics.

with an explicitly factorized transport velocity, decomposing it into N factor-aligned components that capture complementary semantic factors. This design encourages factor-wise separation in the learned representation and enables targeted interventions at generation time by manipulating individual velocity components.

Overview. Given an image I , we encode it into a latent target $\mathbf{z}_1 = E(I)$ using a pretrained VQ-GAN encoder (Van Den Oord et al., 2017). This mapping induces a compact, semantically meaningful latent space and provides a stable training target, improving both efficiency and optimization stability. We then cast image generation as a *transport problem* in this latent space: starting from a simple prior sample, we learn a dynamics that moves the latent state toward \mathbf{z}_1 . To provide structured semantic cues that can steer this transport, we extract a set of N factors with a trainable factor encoder $T_\gamma(\cdot)$,

$$S_\gamma(I) = \{s_i\}_{i=1}^N = T_\gamma(I). \quad (9)$$

Rather than using these factors as a single global condition, we inject them into the flow network via *cross-attention*, which explicitly bridges the flow network with the image encoder through factor-level interactions. Concretely, at multiple U-Net layers, we project intermediate feature maps to queries and attend over $S_\gamma(I)$ as keys and values, allowing the model to retrieve factor-specific information *when and where* it is needed. This cross-attention interface provides a structured conditioning pathway and has been shown to promote semantically aligned generation in prior work (Rombach et al., 2022; Yang et al., 2024).

With this conditioning in place, we learn a factor-conditioned vector field $\mathbf{v}_\theta(\mathbf{z}, S_\gamma(I), t)$ that specifies how a latent state should move at time t . Although flow matching is highly effective for generative modeling, its objective constrains only the *total* velocity to match the target direction and provides no explicit signal for disentangling factor-wise contributions. Consequently, multiple factors can redundantly account for overlapping portions of the transport. To obtain a more interpretable and controllable representation, we factorize the predicted velocity into N factor-aligned components and regularize them to be non-overlapping, so that distinct semantic variations are routed to different factor channels. During training, we jointly optimize network parameters θ and γ , thereby learning disentangled factor-aligned representations. Figure 2 illustrates the overall framework of our method.

4.1. Flow Matching Objective

To train the factor-conditioned vector field \mathbf{v}_θ , we adopt flow matching framework and construct a regression target along a predefined interpolation path connecting a source prior sample to the data latent, conditioned on the factors $S_\gamma(I)$. Concretely, we sample $\mathbf{z}_0 \sim \mathcal{N}(0, \mathbf{I})$ and $t \sim \mathcal{U}[0, 1]$, and define the linear interpolation (as in Eq. (6)):

$$\mathbf{z}_t = (1 - t)\mathbf{z}_0 + t\mathbf{z}_1. \quad (10)$$

This path induces a constant target velocity (cf. Eq. (7)):

$$\mathbf{u}(\mathbf{z}_t, t) = \frac{d\mathbf{z}_t}{dt} = \mathbf{z}_1 - \mathbf{z}_0. \quad (11)$$

We implement \mathbf{v}_θ with a U-Net backbone, and inject the conditioning factors $S_\gamma(I)$ into its intermediate feature representations via cross-attention. Concretely, for a spatial feature map in the U-Net, we form queries from the spatial features and use the factors as keys and values. The cross-attention is defined as

$$\text{Attention}(\mathbf{Q}, \mathbf{K}, \mathbf{V}) = \text{softmax}\left(\frac{\mathbf{Q}\mathbf{K}^\top}{\sqrt{d}}\right)\mathbf{V}, \quad (12)$$

where d is the key/query dimensionality. Substituting the target velocity into the flow matching loss in Eq. (8) yields our factor-conditioned regression objective:

$$\mathcal{L}_{\text{FM}}(\theta) = \mathbb{E}_{t, \mathbf{z}_0, \mathbf{z}_1} \left[\left\| \mathbf{v}_\theta(\mathbf{z}_t, S_\gamma(I), t) - (\mathbf{z}_1 - \mathbf{z}_0) \right\|_2^2 \right]. \quad (13)$$

Why factorization is needed. Although the cross-attention mechanism injects encoder features into \mathbf{v}_θ as semantic context to associate input cues with latent transport, *the flow-matching objective itself does not encourage disentanglement*. It constrains only the aggregate velocity to match the target direction ($\mathbf{z}_1 - \mathbf{z}_0$), without prescribing how individual factors should contribute. Consequently, different factors may redundantly explain the same transport dynamics (e.g., through channel redundancy or cross-factor leakage), resulting in ambiguous attribution and limited controllability. To obtain a factor-aligned and non-redundant decomposition, we explicitly decompose the predicted velocity into factor-specific components and introduce a regularizer that promotes diversity among them.

4.2. Factorized Velocity via Output Attention

We decompose the aggregate velocity field into factor-specific components and encourage them to be non-redundant via an orthogonality regularizer. In practice, we implement this factorization with an output-attention routing mask that, at each spatial location, distributes the predicted velocity across factors by assigning each factor a proportional share.

Factorized velocity and regularization. We decompose the factor-conditioned velocity field as

$$\mathbf{v}_\theta(\mathbf{z}_t, S_\gamma(I), t) = \sum_{i=1}^N \mathbf{v}_\theta^{(i)}(\mathbf{z}_t, S_\gamma(I), t), \quad (14)$$

where $\mathbf{v}_\theta^{(i)}$ denotes the component attributed to the i -th factor. The flow-matching loss $\mathcal{L}_{\text{FM}}(\theta)$ in Eq. (13) is applied to the aggregate field \mathbf{v}_θ ; the regularizer below specifies how the aggregate should be partitioned across factors.

To discourage redundant attributions, we penalize pairwise alignment between factor-specific components. For each

training sample (and each sampled t), we flatten each component into a vector

$$\alpha_i = \text{vec}\left(\mathbf{v}_\theta^{(i)}(\mathbf{z}_t, S_\gamma(I), t)\right), \quad (15)$$

and define the orthogonality loss as the average squared cosine similarity over all factor pairs,

$$\mathcal{L}_{\text{orth}} = \frac{1}{N(N-1)} \sum_{i \neq j} \left(\frac{\alpha_i^\top \alpha_j}{\|\alpha_i\|_2 \|\alpha_j\|_2 + \varepsilon} \right)^2, \quad (16)$$

where ε is a small constant for numerical stability. Minimizing $\mathcal{L}_{\text{orth}}$ encourages different factors to capture distinct transport directions, thereby reducing redundancy and cross-factor leakage.

Practical implementation via output attention. We instantiate $\{\mathbf{v}_\theta^{(i)}\}_{i=1}^N$ using an output-attention routing mask. Let h denote the final hidden feature map produced by the U-Net backbone that predicts \mathbf{v}_θ . We form per-location queries and token keys as

$$\mathbf{Q} = \mathbf{W}_q h, \quad \mathbf{K}_i = \mathbf{W}_k s_i, \quad (17)$$

where \mathbf{W}_q and \mathbf{W}_k are learned projections and d is the key/query dimensionality. The routing weight for factor i is

$$\text{Attn}_i = \frac{\exp\left(\frac{\mathbf{Q}\mathbf{K}_i^\top}{\sqrt{d}}\right)}{\sum_{j=1}^N \exp\left(\frac{\mathbf{Q}\mathbf{K}_j^\top}{\sqrt{d}}\right)}, \quad (18)$$

which satisfies $\sum_{i=1}^N \text{Attn}_i = 1$ at each spatial location. We then define factor-specific velocities by gating the aggregate prediction:

$$\mathbf{v}_\theta^{(i)}(\mathbf{z}_t, S_\phi(I), t) = \text{Attn}_i \odot \mathbf{v}_\theta(\mathbf{z}_t, S_\phi(I), t), \quad (19)$$

where \odot denotes element-wise multiplication (with Attn_i broadcast to match the shape of \mathbf{v}_θ). By the simplex constraint in Eq. (18), the components sum exactly to the aggregate field, recovering Eq. (14).

Why output attention? This design offers three practical advantages: (i) *Factor-aligned attribution*: Attn_i provides an explicit, spatially varying assignment of the velocity field to each factor. (ii) *Mass conservation*: the simplex constraint $\sum_i \text{Attn}_i = 1$ guarantees that the factor-specific components sum exactly to the aggregate prediction, preserving the flow-matching supervision. (iii) *Efficiency and stability*: gating reuses the already-computed aggregate field and adds minimal overhead, while the orthogonality loss in Eq. (16) directly discourages redundant factor routes.

Overall objective. We optimize the combined objective

$$\mathcal{L}(\theta, \phi) = \mathcal{L}_{\text{FM}}(\theta) + \lambda_{\text{orth}} \mathcal{L}_{\text{orth}}, \quad (20)$$

where λ_{orth} controls the strength of the non-redundancy regularization, and we jointly optimize θ and γ .

Table 1. Quantitative comparison on Cars3D, Shapes3D, and MPI3D-toy datasets using FactorVAE score and DCI (mean \pm std).

Method	Cars3D		Shapes3D		MPI3D-toy	
	FactorVAE \uparrow	DCI \uparrow	FactorVAE \uparrow	DCI \uparrow	FactorVAE \uparrow	DCI \uparrow
VAE	FactorVAE	0.906 \pm 0.052	0.161 \pm 0.019	0.840 \pm 0.066	0.611 \pm 0.101	0.152 \pm 0.025
	β -TCVAE	0.855 \pm 0.082	0.140 \pm 0.019	0.873 \pm 0.074	0.613 \pm 0.114	0.179 \pm 0.017
	DAVA	0.940 \pm 0.010	0.230 \pm 0.040	0.820 \pm 0.030	0.780 \pm 0.030	0.410 \pm 0.040
GAN	ClosedForm	0.873 \pm 0.036	0.243 \pm 0.048	0.951 \pm 0.021	0.525 \pm 0.078	0.523 \pm 0.056
	GANSpace	0.932 \pm 0.018	0.209 \pm 0.031	0.788 \pm 0.091	0.284 \pm 0.034	0.465 \pm 0.036
	Disco-GAN	0.855 \pm 0.074	0.271 \pm 0.037	0.877 \pm 0.031	0.708 \pm 0.048	0.371 \pm 0.030
Diffusion	DisDiff	0.976 \pm 0.018	0.232 \pm 0.019	0.902 \pm 0.043	0.723 \pm 0.013	0.617 \pm 0.070
	FDAE	0.912 \pm 0.020	0.329 \pm 0.061	0.998 \pm 0.003	0.762 \pm 0.064	0.756 \pm 0.071
	EncDiff	0.948 \pm 0.017	0.357 \pm 0.072	0.999 \pm 0.001	0.952 \pm 0.028	0.862 \pm 0.026
	DyGA	0.846 \pm 0.015	0.307 \pm 0.032	0.958 \pm 0.044	0.833 \pm 0.054	0.732 \pm 0.051
Ours		0.964 \pm 0.013	0.431 \pm 0.034	1.000 \pm 0.000	0.973 \pm 0.020	0.907 \pm 0.017
						0.649 \pm 0.024

Choice of λ_{orth} . In practice, we select λ_{orth} via a small validation sweep over $\{10^{-4}, 10^{-3}, 10^{-2}, 10^{-1}, 0\}$ and choose the largest value that improves factor diversity without degrading \mathcal{L}_{FM} or sample quality. We use $\lambda_{\text{orth}} = 10^{-2}$ in all experiments.

5. Experiments

In this section, we present both qualitative and quantitative results that demonstrate the effectiveness of our method on both synthetic and real-world data. All experiments are conducted on a Linux server equipped with $8 \times$ NVIDIA RTX 4090 GPUs. The code will be released upon publication.

5.1. Experimental Setup

Datasets. We evaluate on standard disentanglement datasets: Cars3D (Reed et al., 2015), Shapes3D (Sun et al., 2018), and MPI3D-toy (Gondal et al., 2019). Cars3D comprises 3D-rendered car images with viewpoint-related factors. Shapes3D consists of procedurally rendered 3D objects with multiple controlled generative factors (e.g., shape, size, orientation, and color). MPI3D-toy contains images rendered in a controlled environment with annotated factors of variation. To assess performance on real-world imagery, we additionally report results on CelebA (Liu et al., 2015), a large-scale face dataset with attribute annotations.

Baselines. We compare against three families of baselines. *VAE-based*: FactorVAE (Kim & Mnih, 2018), β -TCVAE (Chen et al., 2018), and DAVA (Estermann & Wattenhofer, 2023). *GAN-based*: ClosedForm (Shen & Zhou, 2021), GANSpace (Härkönen et al., 2020), and DisCoGAN (Ren et al., 2022). *Diffusion-based*: DisDiff (Yang et al., 2023b), FDAE (Wu & Zheng, 2024), EncDiff (Yang et al., 2024), and DyGA (Jun et al., 2025). We use official implementations when available; otherwise, we implement each method following the original paper. Across methods,

we keep preprocessing, training budget (steps/epochs), and model capacity as consistent as possible.

Evaluation metrics. On synthetic datasets with ground-truth generative factors, we report the FactorVAE score (Kim & Mnih, 2018) and DCI disentanglement (Eastwood & Williams, 2018). We use these as primary metrics because they offer complementary views of disentanglement with limited redundancy, consistent with prior observations on metric covariance (Locatello et al., 2019): the FactorVAE score measures factor-to-dimension alignment, while DCI disentanglement captures dimension-wise specificity (Eastwood & Williams, 2018). For CelebA, where ground-truth generative factors are not available in the same form, we report TAD (Yeats et al., 2022) to evaluate attribute-level controllability and leakage (changing a target attribute with minimal unintended changes), and Fréchet Inception Distance (FID) (Heusel et al., 2017) to assess sample quality and distributional fidelity. Following common practice, we compute all metrics except FID on a PCA-reduced latent representation when the learned latent is high-dimensional, consistent with prior evaluations.

Implementation details. Across all datasets, we train the model with a batch size of 128. Following (Locatello et al., 2019), we fix the number of generative factors to 10 for each dataset. During sampling, we solve the associated ODE using the adaptive-step Dopr5 solver (Akhtar, 2025). All reported results are averaged over 10 independent runs.

5.2. Comparison with the State-of-the-art Methods

Here, we quantitatively compare our method against existing disentangled representation learning methods.

Results: Cars3D, Shapes3D, and MPI3D-toy. Table 1 evaluates disentanglement on three synthetic datasets using FactorVAE score and DCI disentanglement metrics. We

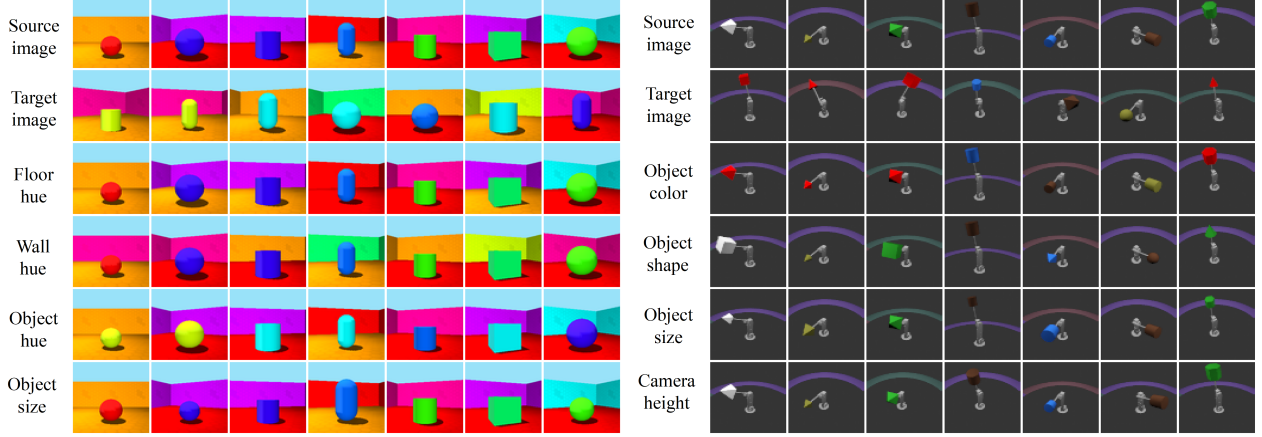


Figure 3. Factor swapping results. Conditional generation results obtained by intervening on a single latent unit. For each pair of images, we encode a *source* and a *target*, replace one latent unit in the source code with the corresponding unit from the target, and generate from the modified representation. The first two rows show the source and target images, respectively; rows three to six show the source image with only the swapped attribute (e.g., Wall hue, Object shape) transferred from the target. Left: Shapes3D. Right: MPI3D-toy.

observe a clear hierarchy: our method substantially outperforms VAE- and GAN-based methods, and yields consistent (though smaller) gains over recent diffusion-based methods. Compared to VAE- and GAN-based baselines, our method yields substantial gains across all datasets, with the most pronounced improvements on the FactorVAE score and DCI disentanglement. For example, on MPI3D-toy dataset our method achieves **0.907** FactorVAE score and **0.649** DCI disentanglement, outperforming the strongest VAE-based method (DAVA: **0.410** FactorVAE and **0.300** DCI) and the strongest GAN-based method (ClosedForm: **0.523** FactorVAE and **0.318** DCI). A plausible explanation is that standard VAEs must trade off reconstruction fidelity against factorized latents under a restrictive likelihood model and KL regularization, often resulting in either entangled representations or reduced information content. GAN-based latent discovery methods that lack explicit encoder-generator alignment can yield unstable directions that do not reliably correspond to individual generative factors. By learning a flow-matching vector field that induces a coherent generative trajectory over time, our method achieves consistently higher FactorVAE and DCI values. Compared to diffusion-based baselines, the gains are smaller but consistent. We attribute this to the fact that diffusion models already provide a strong generative backbone, so remaining gains depend on how effectively a method enforces semantic coordinate structure in the latent space. Our method strengthens this alignment by explicitly promoting factor-aligned latent structure, leading to higher DCI without sacrificing the FactorVAE score.

Results: CelebA. Table 2 reports disentanglement-related behavior ($TAD \uparrow$) and sample quality ($FID \downarrow$) on the CelebA dataset. Our method achieves the best performance on both

metrics, consistently indicating superior attribute-level controllability with reduced leakage, while simultaneously producing visually higher-fidelity samples. Collectively, these results demonstrate that the benefits of our method extend beyond synthetic datasets and generalize effectively to realistic and complex image distributions.

Table 2. Comparison of disentanglement and generation quality using the TAD and FID metrics (mean \pm std) on CelebA dataset.

Method	TAD \uparrow	FID \downarrow
FactorVAE	0.148 ± 0.031	97.6 ± 1.8
DisDiff	0.305 ± 0.010	18.2 ± 2.1
FDAE	0.326 ± 0.044	19.0 ± 1.6
EncDiff	0.638 ± 0.008	14.8 ± 2.3
DyGA	0.954 ± 0.024	12.0 ± 1.2
Ours	1.154 ± 0.089	8.1 ± 0.2

5.3. Visualization Results

A simple yet effective way to evaluate whether the feature extractor learns *well-disentangled* representations is to actively intervene on the inferred factors and inspect the resulting generations. If changing a single factor induces a predictable, semantically coherent modification in the output while leaving other attributes largely unchanged, this indicates that the representation separates underlying generative factors (Bengio et al., 2013). We therefore perform a *factor swapping* experiment. Given two distinct images, we encode each into its set of factors, swap one factor between the two codes, and then synthesize images conditioned on the swapped representations. Evidence of disentanglement is provided when the exchanged factor transfers only the intended attribute (e.g., Wall hue, Object shape) from one image to the other without causing collateral changes in un-

Table 3. Ablation results on the Cars3D, Shapes3D, and MPI3D-toy datasets.

Method	Cars3D		Shapes3D		MPI3D-toy	
	FactorVAE \uparrow	DCI \uparrow	FactorVAE \uparrow	DCI \uparrow	FactorVAE \uparrow	DCI \uparrow
\mathcal{L}_{FM}	0.944 \pm 0.034	0.414 \pm 0.029	0.999 \pm 0.001	0.961 \pm 0.026	0.745 \pm 0.031	0.571 \pm 0.062
$\mathcal{L}_{\text{FM}} + \mathcal{L}_{\text{orth}}$	0.964 \pm 0.013	0.431 \pm 0.034	1.000 \pm 0.000	0.973 \pm 0.020	0.907 \pm 0.017	0.649 \pm 0.024

Table 4. Statistical efficiency in learning a GBT-based downstream task on Shapes3D and MPI3D-toy datasets.

Method	Shapes3D		MPI3D-toy	
	Acc ₁₀₀₀ /Acc	Acc ₁₀₀ /Acc	Acc ₁₀₀₀ /Acc	Acc ₁₀₀ /Acc
DisDiff	0.928 \pm 0.001	0.732 \pm 0.002	0.862 \pm 0.001	0.700 \pm 0.002
FDAE	0.983 \pm 0.004	0.746 \pm 0.004	0.847 \pm 0.011	0.745 \pm 0.012
EncDiff	0.975 \pm 0.000	0.772 \pm 0.002	0.853 \pm 0.005	0.701 \pm 0.001
DyGA	0.961 \pm 0.033	0.800 \pm 0.066	0.896 \pm 0.032	0.750 \pm 0.028
Ours	0.993 \pm 0.001	0.908 \pm 0.020	0.907 \pm 0.008	0.752 \pm 0.034

related factors. We focus on the Shapes3D and MPI3D-toy datasets and report qualitative results in Figure 3. Overall, our method faithfully captures subtle factor variations and enables precise, consistent factor-level control, indicating strong disentanglement alongside high-quality generation.

5.4. Ablation Study

To quantify the effect of the proposed orthogonality regularizer $\mathcal{L}_{\text{orth}}$, we conduct an ablation study comparing the base flow matching objective $\mathcal{L}_{\text{FM}}(\theta)$ with its regularized variant, while keeping the architecture, training schedule, and all hyperparameters unchanged. As shown in Table 3, adding $\mathcal{L}_{\text{orth}}$ yields consistent improvements on these datasets. These results indicate that $\mathcal{L}_{\text{orth}}$ plays a key role in promoting factor separation: it discourages different factor tokens from encoding redundant information, leading to more disentangled representations and more reliable factor-level control, especially in the more challenging MPI3D-toy setting.

5.5. Downstream Tasks

Disentangled representations are commonly evaluated through their effectiveness on downstream machine learning tasks. To verify the practical utility of our learned representations, we follow the evaluation protocol proposed in (Jun et al., 2025) and assess learning efficiency using Gradient Boosted Trees (GBT). Specifically, we consider a downstream classification task in which classifiers are trained on the learned representations using limited numbers of labeled samples. We report two accuracy metrics, Acc₁₀₀₀ and Acc₁₀₀, corresponding to training with 1,000 and 100 labeled samples, respectively, and compare them against Acc, obtained using 10,000 labeled samples. This evaluation measures how effectively the learned representations support sample-efficient learning under data-scarce conditions. For comparison, we include representative baseline methods

from prior work DisDiff (Yang et al., 2023b), Fdae (Wu & Zheng, 2024), EncDiff (Yang et al., 2024), and DyGA (Jun et al., 2025). The quantitative results are summarized in Table 4. As shown, our method consistently outperforms all baselines across both datasets. These results indicate that the representations learned by our method are more informative and sample-efficient, supporting the view that factor-wise disentanglement provides a beneficial inductive bias for effective downstream learning.

6. Conclusion

We present a flow-matching-based approach to disentangled representation learning that casts disentanglement as factor-conditioned transport in a compact latent space. By modeling generation through deterministic flows and introducing an orthogonality regularizer, our method explicitly promotes semantic alignment while mitigating cross-factor interference. Empirical results across multiple datasets demonstrate that the proposed method consistently improves disentanglement quality (e.g., DCI and FactorVAE), controllability, and sample fidelity compared to representative diffusion-based baselines. Our results suggest that viewing representation learning through the lens of structured latent transport opens a new and promising direction for disentanglement, offering a fundamentally different alternative to noise-driven diffusion dynamics.

Impact Statement

This paper presents work whose goal is to advance the field of Machine Learning. There are many potential societal consequences of our work, none of which we feel must be specifically highlighted here.

References

Akhtar, S. W. On tuning neural ODE for stability, consistency and faster convergence. *SN Computer Science*, 6(4):318, 2025.

Bengio, Y., Courville, A., and Vincent, P. Representation learning: A review and new perspectives. *IEEE Transactions on Pattern Analysis and Machine Intelligence*, 35(8):1798–1828, 2013.

Burgess, C. P., Higgins, I., Pal, A., Matthey, L., Watters, N., Desjardins, G., and Lerchner, A. Understanding disentangling in beta-vae. *arXiv preprint arXiv:1804.03599*, 2018.

Chen, R. T., Li, X., Grosse, R. B., and Duvenaud, D. K. Isolating sources of disentanglement in variational autoencoders. In *Neural Information Processing Systems*, pp. 2610–2620, 2018.

Chen, X., Duan, Y., Houthooft, R., Schulman, J., Sutskever, I., and Abbeel, P. Infogan: Interpretable representation learning by information maximizing generative adversarial nets. In *Neural Information Processing Systems*, pp. 2172–2180, 2016.

Cheng, P., Min, M. R., Shen, D., Malon, C., Zhang, Y., Li, Y., and Carin, L. Improving disentangled text representation learning with information-theoretic guidance. In *Association for Computational Linguistics*, pp. 7530–7541, 2020.

Dao, Q., Phung, H., Nguyen, B., and Tran, A. Flow matching in latent space. *arXiv preprint arXiv:2307.08698*, 2023.

Eastwood, C. and Williams, C. K. A framework for the quantitative evaluation of disentangled representations. In *International Conference on Learning Representations*, 2018.

Estermann, B. and Wattenhofer, R. Dava: Disentangling adversarial variational autoencoder. In *International Conference on Learning Representations*, 2023.

Gondal, M. W., Wuthrich, M., Miladinovic, D., Locatello, F., Breidt, M., Volchkov, V., Akpo, J., Bachem, O., Schölkopf, B., and Bauer, S. On the transfer of inductive bias from simulation to the real world: a new disentanglement dataset. In *Neural Information Processing Systems*, volume 32, 2019.

Goodfellow, I., Pouget-Abadie, J., Mirza, M., Xu, B., Warde-Farley, D., Ozair, S., Courville, A., and Bengio, Y. Generative adversarial nets. In *Neural Information Processing Systems*, 2014.

Härkönen, E., Hertzmann, A., Lehtinen, J., and Paris, S. Ganspace: Discovering interpretable gan controls. In *Neural Information Processing Systems*, volume 33, pp. 9841–9850, 2020.

Heusel, M., Ramsauer, H., Unterthiner, T., Nessler, B., and Hochreiter, S. Gans trained by a two time-scale update rule converge to a local nash equilibrium. In *Neural Information Processing Systems*, volume 30, 2017.

Higgins, I., Matthey, L., Pal, A., Burgess, C., Glorot, X., Botvinick, M., Mohamed, S., and Lerchner, A. betavae: Learning basic visual concepts with a constrained variational framework. In *International Conference on Learning Representations*, 2017.

Higgins, I., Amos, D., Pfau, D., Racaniere, S., Matthey, L., Rezende, D., and Lerchner, A. Towards a definition of disentangled representations. *arXiv preprint arXiv:1812.02230*, 2018.

Ho, J., Jain, A., and Abbeel, P. Denoising diffusion probabilistic models. In *Neural Information Processing Systems*, volume 33, pp. 6840–6851, 2020.

Hu, Z., Lee, R. K.-W., Aggarwal, C. C., and Zhang, A. Text style transfer: A review and experimental evaluation. *ACM SIGKDD Explorations Newsletter*, 24(1):14–45, 2022.

Jun, Y., Park, J., Choo, K., Choi, T. E., and Hwang, S. J. Disentangling disentangled representations: Towards improved latent units via diffusion models. In *Winter Conference on Applications of Computer Vision*, pp. 3559–3569, 2025.

Karras, T., Laine, S., and Aila, T. A style-based generator architecture for generative adversarial networks. In *Computer Vision and Pattern Recognition*, pp. 4401–4410, 2019.

Karras, T., Laine, S., Aittala, M., Hellsten, J., Lehtinen, J., and Aila, T. Analyzing and improving the image quality of stylegan. In *Computer Vision and Pattern Recognition*, pp. 8110–8119, 2020.

Kazemi, H., Iranmanesh, S. M., and Nasrabadi, N. Style and content disentanglement in generative adversarial networks. In *IEEE Winter Conference on Applications of Computer Vision*, pp. 848–856, 2019.

Kim, H. and Mnih, A. Disentangling by factorising. In *International Conference on Machine Learning*, pp. 2649–2658, 2018.

Kingma, D. P. and Welling, M. Auto-encoding variational bayes. In *International Conference on Learning Representations*, 2014.

Kumar, A., Sattigeri, P., and Balakrishnan, A. Variational inference of disentangled latent concepts from unlabeled observations. In *International Conference on Learning Representations*, 2018.

Lin, Z., Thekumparampil, K., Fanti, G., and Oh, S. Infogan-cr and modelcentrality: Self-supervised model training and selection for disentangling gans. In *International Conference on Machine Learning*, pp. 6127–6139, 2020.

Lipman, Y., Chen, R. T., Ben-Hamu, H., Nickel, M., and Le, M. Flow matching for generative modeling. *arXiv preprint arXiv:2210.02747*, 2022.

Liu, Z., Luo, P., Wang, X., and Tang, X. Deep learning face attributes in the wild. In *International Conference on Computer Vision*, pp. 3730–3738, 2015.

Locatello, F., Bauer, S., Lucic, M., Raetsch, G., Gelly, S., Schölkopf, B., and Bachem, O. Challenging common assumptions in the unsupervised learning of disentangled representations. In *International Conference on Machine Learning*, pp. 4114–4124, 2019.

Reed, S. E., Zhang, Y., Zhang, Y., and Lee, H. Deep visual analogy-making. In *Neural Information Processing Systems*, volume 28, 2015.

Ren, X., Yang, T., Wang, Y., and Zeng, W. Learning disentangled representation by exploiting pretrained generative models: A contrastive learning view. In *International Conference on Learning Representations*, 2022.

Rombach, R., Blattmann, A., Lorenz, D., Esser, P., and Ommer, B. High-resolution image synthesis with latent diffusion models. In *Computer Vision and Pattern Recognition*, pp. 10684–10695, 2022.

Shen, Y. and Zhou, B. Closed-form factorization of latent semantics in gans. In *Computer Vision and Pattern Recognition*, pp. 1532–1540, 2021.

Sun, X., Wu, J., Zhang, X., Zhang, Z., Zhang, C., Xue, T., Tenenbaum, J. B., and Freeman, W. T. Pix3d: Dataset and methods for single-image 3d shape modeling. In *Computer Vision and Pattern Recognition*, pp. 2974–2983, 2018.

Van Den Oord, A., Vinyals, O., et al. Neural discrete representation learning. In *Neural Information Processing Systems*, volume 30, 2017.

Varur, S., Hanchinamani, A. R., Bagewadi, T. S., Mudenagudi, U., Desai, C. D., Desai, P., Meharwade, S., et al. Disc-gan: Disentangling style and content for cluster-specific synthetic underwater image generation. In *International Conference on Computer Vision*, pp. 6844–6852, 2025.

Wang, D., Deng, Y., Yin, Z., Shum, H.-Y., and Wang, B. Progressive disentangled representation learning for fine-grained controllable talking head synthesis. In *Computer Vision and Pattern Recognition*, pp. 17979–17989, 2023.

Wang, T., Zhang, Y., Fan, Y., Wang, J., and Chen, Q. High-fidelity gan inversion for image attribute editing. In *Computer Vision and Pattern Recognition*, pp. 11379–11388, 2022.

Wang, X., Chen, H., Tang, S., Wu, Z., and Zhu, W. Disentangled representation learning. *IEEE Transactions on Pattern Analysis and Machine Intelligence*, 46(12): 9677–9696, 2024.

Wu, A. and Zheng, W.-S. Factorized diffusion autoencoder for unsupervised disentangled representation learning. In *Proceedings of the AAAI Conference on Artificial Intelligence*, volume 38, pp. 5930–5939, 2024.

Wu, K., Zhu, Y., Li, J., Wen, J., Liu, N., Xu, Z., and Tang, J. Discrete policy: Learning disentangled action space for multi-task robotic manipulation. In *International Conference on Robotics and Automation*, pp. 8811–8818, 2025.

Xu, Y., Chai, M., Shi, Z., Peng, S., Skorokhodov, I., Siarohin, A., Yang, C., Shen, Y., Lee, H.-Y., Zhou, B., et al. Discoscene: Spatially disentangled generative radiance fields for controllable 3d-aware scene synthesis. In *Computer Vision and Pattern Recognition*, pp. 4402–4412, 2023.

Yang, L., Zhang, Z., Song, Y., Hong, S., Xu, R., Zhao, Y., Zhang, W., Cui, B., and Yang, M.-H. Diffusion models: A comprehensive survey of methods and applications. *ACM Computing Surveys*, 56(4):1–39, 2023a.

Yang, T., Wang, Y., Lu, Y., and Zheng, N. Disdiff: Unsupervised disentanglement of diffusion probabilistic models. In *Neural Information Processing Systems*, volume 36, pp. 69130–69156, 2023b.

Yang, T., Lan, C., Lu, Y., and Zheng, N. Diffusion model with cross attention as an inductive bias for disentanglement. In *Neural Information Processing Systems*, volume 37, pp. 82465–82492, 2024.

Yeats, E., Liu, F., Womble, D., and Li, H. Nashae: Disentangling representations through adversarial covariance minimization. In *European Conference on Computer Vision*, pp. 36–51, 2022.

A. More Implementation Details

A.1. Algorithm

Here, we present the overall algorithm for learning disentangled representations within the flow matching framework.

Algorithm 1 Overall Disentangled Representation Learning Framework

- 1: **Input:** pretrained VQ-VAE encoder $E(\cdot)$, neural networks T_γ and \mathbf{v}_θ , number of factors N , orthogonality weight λ_{orth}
- 2: **Setting:** Random initialization of model parameters θ, γ
- 3: **While** not converged
- 4: Sample an image I from the training set
- 5: Encode the image to latent space: $\mathbf{z}_1 \leftarrow E(I)$
- 6: Extract factor tokens: $S_\gamma(I) = \{s_i\}_{i=1}^N \leftarrow T_\gamma(I)$
- 7: Sample prior latent $\mathbf{z}_0 \sim \mathcal{N}(0, \mathbf{I})$ and time $t \sim \mathcal{U}[0, 1]$
- 8: Construct interpolation: $\mathbf{z}_t \leftarrow (1 - t)\mathbf{z}_0 + t\mathbf{z}_1$
- 9: Compute target velocity: $\mathbf{u} \leftarrow \mathbf{z}_1 - \mathbf{z}_0$
- 10: Predict aggregate velocity with cross-attention conditioning $\mathbf{v}_\theta(\mathbf{z}_t, S_\gamma(I), t)$ via U-Net backbone
- 11: Compute output-attention routing weights $\{\text{Attn}_i\}_{i=1}^N$ using Eq. (18)
- 12: Obtain factor-specific velocities: $\mathbf{v}_\theta^{(i)} \leftarrow \text{Attn}_i \odot \mathbf{v}_\theta$
- 13: Compute flow matching loss: $\mathcal{L}_{\text{FM}} \leftarrow \|\mathbf{v}_\theta - \mathbf{u}\|_2^2$
- 14: Compute orthogonality regularizer $\mathcal{L}_{\text{orth}}$ using Eq. (16)
- 15: Update parameters: $(\theta, \gamma) \leftarrow \nabla(\mathcal{L}_{\text{FM}} + \lambda_{\text{orth}}\mathcal{L}_{\text{orth}})$
- 16: **EndWhile**
- 17: **Output:** θ, γ

A.2. Model Architecture

For fair comparison, we adopt the same image encoder architecture as EncDiff (Yang et al., 2024) for extracting generative factors. The encoder follows a convolutional backbone with progressive downsampling and fully connected layers, as detailed below.

Table 5. Architecture of the Image Encoder for Factor Extraction

Layer Configuration
Conv 7×7 , $3 \rightarrow 64$, stride = 1
ReLU
Conv 4×4 , $64 \rightarrow 128$, stride = 2
ReLU
Conv 4×4 , $128 \rightarrow 256$, stride = 2
ReLU
Conv 4×4 , $256 \rightarrow 256$, stride = 2
ReLU
Conv 4×4 , $256 \rightarrow 256$, stride = 2
ReLU
FC $4096 \rightarrow 256$
ReLU
FC $256 \rightarrow 256$
ReLU
FC $256 \rightarrow K$

For the velocity prediction network, we adopt a U-Net architecture. The detailed configuration for different datasets is summarized in Table 6.

Table 6. U-Net architecture and training configuration for velocity prediction.

Parameters	Shapes3D / Cars3D / MPI3D-toy / CelebA
Base channels	16
Channel multipliers	[1, 2, 4, 4]
Attention resolutions	[1, 2, 4]
Number of attention heads	8
Model channels	64
Dropout	0.1
Images trained	0.48M / 0.28M / 1.03M / 0.20M

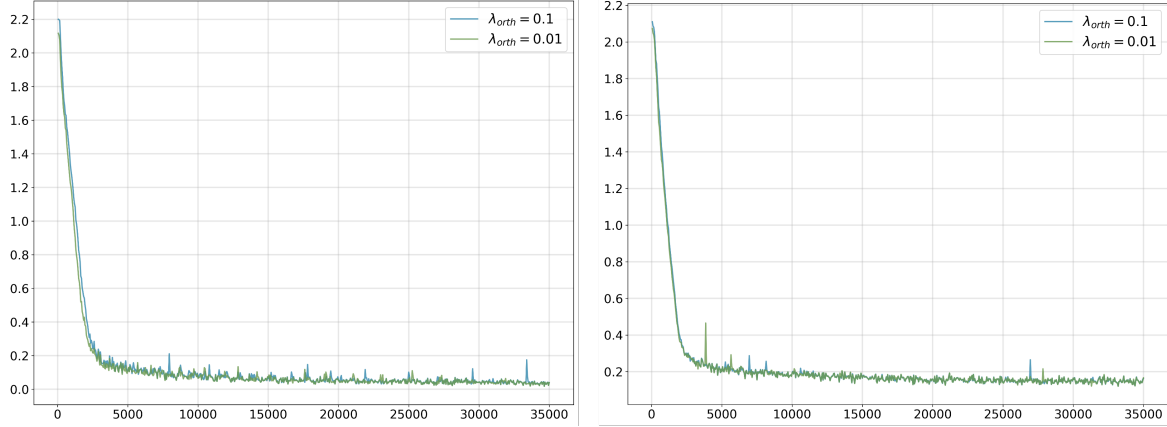


Figure 4. Training loss curves. Left: Shapes3D. Right: MPI3D-toy.

A.3. More Experiments

More metrics results. We conduct a comprehensive evaluation of disentanglement performance not only the FactorVAE score and DCI disentanglement, but also an additional metric Mutual Information Gap (MIG). The results are shown in Table 7.

Table 7. Results for more metrics on Cars3D, Shapes3D and MPI3D-toy datasets.

Dataset	FactorVAE score↑	DCI↑	MIG↑
Cars3D	0.964 ± 0.013	0.431 ± 0.034	0.139 ± 0.018
Shapes3D	1.000 ± 0.000	0.973 ± 0.020	0.509 ± 0.036
MPI3D-toy	0.907 ± 0.017	0.649 ± 0.024	0.431 ± 0.059

Training loss curve. We visualize the training loss curves for different settings of the hyperparameter λ . As shown in Figure 4, our method exhibits stable and consistent convergence across all configurations.